Biosensors and Bioelectronics 25 (2010) 2259–2264

Contents lists available at ScienceDirect

Biosensors and Bioelectronics

journal homepage: www.elsevier.com/locate/bios

Low-cost, transparent, and flexible single-walled carbon nanotube nanocomposite based ion-sensitive field-effect transistors for pH/glucose sensing

Dongjin Lee, Tianhong Cui*

Department of Mechanical Engineering, University of Minnesota at Twin Cities, 111 Church Street S.E., Minneapolis, MN 55455, USA

ARTICLE INFO

Article history:
Received 28 November 2009
Received in revised form 14 February 2010
Accepted 2 March 2010
Available online 27 March 2010

Keywords:
Flexible sensor
Carbon nanotube
Layer-by-layer self-assembly
pH sensor
Glucose sensor
ISFET

ABSTRACT

Low-cost, transparent, and flexible ion-sensitive field-effect transistors (ISFETs) are presented as pH and glucose sensors. Single-walled carbon nanotubes (SWCNTs) and poly(diallyldimethyammonium chloride, PDDA) are deposited by layer-by-layer (LbL) self-assembly between two metallic electrodes patterned on a polyethylene terephthalate substrate. The pH ISFETs are characterized based on the fact that the electronic conductance of SWCNTs nanocomposite is determined by molecular protonation/deprotonation of carboxylic groups on SWCNTs and by the external Ag/AgCl reference gate voltage. Glucose is detected by the local pH change in the vicinity of SWCNTs with the aid of glucose oxidase (GOx) enzyme. The glucose sensor shows a sensitivity of 18–45 μA/mM on a linear range of 2–10 mM. The apparent Michaelis–Menten constant is 14.2 mM, indicating a high affinity of LbL assembled GOx to glucose. The LbL self-assembly of nanomaterials and enzymes on the transparent and flexible substrate suggests various chemical and biological sensors suitable for *in vivo* application.

Published by Elsevier B.V.

1. Introduction

Carbon nanotubes (CNTs) have been of great interest as a functional material for the past two decades due to their extraordinary properties (Han, 2004). To take full advantage of such excellent properties, CNTs need to be integrated into an existing device or a matrix material to be utilized as active components such as electrically conducting wires, semiconducting channel materials for transistors, and sensing elements, etc. Layer-by-layer (LbL) assembly has been used to manufacture ultra-thin film as a functional material with the controlled internal structure of polyelectrolytes (Nohria et al., 2006), CNTs (Mamedov et al., 2002; Xue and Cui, 2008b), nanoparticles (Zeng et al., 2001), and even biomolecules (Shutava et al., 2006) under room temperature and atmospheric pressure. It is environmentally sound and potentially cost-effective. Furthermore, it can be performed on various sizes, shapes, and materials of the substrate (Fujimoto et al., 2005; Jiang and Tsukruk, 2006). Since the pioneering research on LbL assembly of CNTs (Mamedov et al., 2002), much effort has been made to exploit the versatility of the LbL assembled CNTs multilayer, particularly as sensors (Lee and Cui, 2009a; Loh et al., 2007; Xue and Cui, 2008b; Yu et al., 2006a) and actuators (Yu et al., 2006b). Moreover, LbL assembly of CNTs has been coming into the spotlight as an alternative method to integrate CNT into devices or versatile functional materials without any segregation (Rouse and Lillehei, 2003).

There has been much research effort to attain flexible electronics with emphasis on applications like electronic bar codes, RFID tags, smart credit cards, and flexible displays (Bock, 2005). Transparency allows the multilayer packaging such that internal product information is visible, which provides the simplicity of inspection. For this reason, the assembly of nanomaterials on the flexible and transparent substrate, with the capability of selective placement or patterning of the assembled film, is getting more and more important in order to exploit novel properties for the emerging application of not only electronics but also nanoscale physical or chemical sensors. In this report, CNTs were integrated into ISFET sensors as a channel material by LbL assembly and lithographic patterning on the low-cost, transparent and flexible substrate, and pH/glucose sensing applications are demonstrated. The fabrication of metal electrodes and the patterning of LbL assembled SWCNT films were accomplished via the lithographic techniques. After the fabrication of metal electrodes, SWCNTs were self-assembled and patterned as an electrochemical transducer layer using the lift-off. Flexible devices were tested in the various pH buffer solutions on the physiological range to show an ion-sensitive electrochemical property. With the aid of bio-receptors, glucose oxidase (GOx) enzymes, glucose was detected in the same way as pH. The fabricated SWCNT-based flexible ISFET sensor has been proven to be a versatile chemical and biological sensor, which makes *in vivo* application promising due to biocompatible nature of polymer substrate.

* Corresponding author. Tel.: +1 612 626 1636; fax: +1 612 625 6069.
E-mail address: tcui@me.umn.edu (T. Cui).

0956-5663/$ – see front matter. Published by Elsevier B.V.
doi:10.1016/j.bios.2010.03.003

The assembly of nanomaterials on low-cost, transparent, and flexible substrate via LbL bottom-up construction is cost-effective and suggests new paradigm of manufacturing process.

2. Experimental

2.1. Materials

SWCNTs (1–2 nm in diameter, 50 μm in length) were chemically functionalized in the concentrated acid as reported previously (Lee and Cui, 2009a,b), since pristine SWCNTs (p-SWCNT) are generally inappropriate for the LbL assembly due to the poor solubility to water. Subsequently, FTIR showed the C=O stretching vibration peak at 1740 cm^{-1} (Lee and Cui, 2009b), which is a strong indication of the presence of carboxylic groups. The chemical functionalization induced hydrophilic carboxylic functional groups and promoted the solubility and stability of SWCNTs in water (Supplementary Fig. 1). The final concentration of SWCNT solution was about 0.6 mg/ml.

Polyelectrolytes used were poly(diallyldimethyammonium chloride, PDDA, M_w = 200–350k, Aldrich) and poly(styrene-sulfonate, PSS, M_w = 70k, Aldrich). The concentration of PDDA and PSS aqueous solution was 1.4 and 0.3 wt%, respectively, with 0.5 M sodium chloride (NaCl). Glucose oxidase (GOx, Type VII, lyophilized powder, 50 kU/g, from *Aspergillus niger*, Aldrich) was dissolved into 1× phosphate buffered saline (PBS, pH 7.2, GIBCO, KCl: 2.67 mM, KH_2PO_4: 1.47 mM, NaCl: 137.93 mM, $Na_2HPO_4{\cdot}7H_2O$: 8.06 mM) to yield stable negative charges with a concentration of 1 mg/mL. Standard pH buffer solutions used in this study were an aqueous solution of phosphate monobasic (NaH_2PO_4) and dibasic (Na_2HPO_4) on the range of 5–9 with buffering power of 80 mM. Standard β-D-glucose (Aldrich) solutions were prepared by dissolving glucose into 1× PBS.

2.2. Flexible sensor fabrication

The fabrication process of the flexible sensor is depicted in Fig. 1. Polyethylene terephthalate polyester flexible substrate (250 μm thick, 100 mm in diameter) was cleaned in acetone, methanol, and isopropyl alcohol for 5 min, respectively, in order to remove organic contaminants followed by rinsing with deionized water (DIH_2O). Chromium (Cr, 250 Å) and gold (Au, 1000 Å) were sputter-deposited on a freestanding substrate without the intervening of a dielectric layer (Fig. 1a). Photoresist (PR) was applied to make the electrode pattern by photolithography. Following exposure and development (Fig. 1b), Au and Cr were etched out successively (Fig. 1c). The second lithography was used to fabricate the window area through which SWCNTs were assembled between drain and source electrodes to avoid unwanted electrochemical reaction in areas other than channels (Fig. 1d). The surface was treated with oxygen (O_2) plasma at 100 W for 1 min with O_2 flow rate of 100 sccm to remove the residual photoresist and change the surface wettable for the subsequent LbL assembly.

The precursor layer of $(PDDA/PSS)_3$ was assembled for surface charge enhancement. Subsequently, $(PDDA/SWCNT)_3$ was assembled as an electrochemical transducer (Fig. 1e). The dipping time used for polyelectrolytes and SWCNTs is 10 and 15 min, respectively. Lift-off technique was used to remove the LbL assembled film from the areas other than channel (Fig. 1f) in the ultrasonic bath. Additional biomolecular multilayer of $(PDDA/GOx)_3$ was assembled for the glucose detection (Fig. 1g). The final glucose sensor is schematized in Fig. 2a, where close-up thin film hierarchy is shown. This ISFET sensor serves as a pH sensor without (PDDA/GOx) multilayer.

2.3. Electrochemical detection

The electrochemical detection of pH and glucose concentration was performed using the ISFET characterization technique that is depicted in Fig. 2a. The miniaturized Ag/AgCl reference electrode (Cypress Systems, EE008) with internal filling solution of 3 M KCl was immersed into sample solutions as a gate, as shown in Fig. 2b, to provide the sample solution with the stable electrical potential. After three terminals (source, drain, and gate) were connected to the semiconductor parameter analyzer (HP 4156A), drain-to-source voltage (V_{DS}) and gate voltage (V_G) were scanned to obtain drain current (I_D) at different samples solutions.

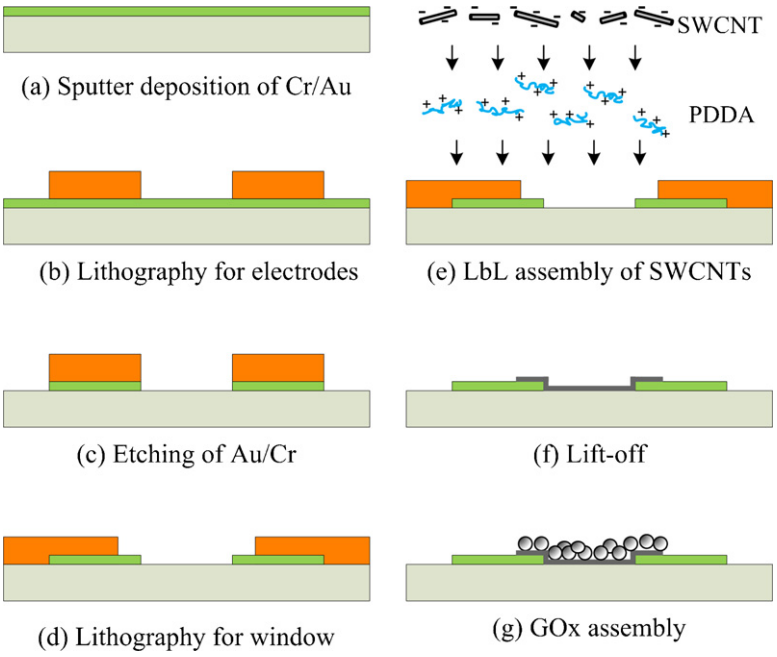

Fig. 1. The fabrication process of flexible SWCNT ISFET sensors: a combination of microfabricated metal electrodes and LbL nano self-assembled SWCNTs.

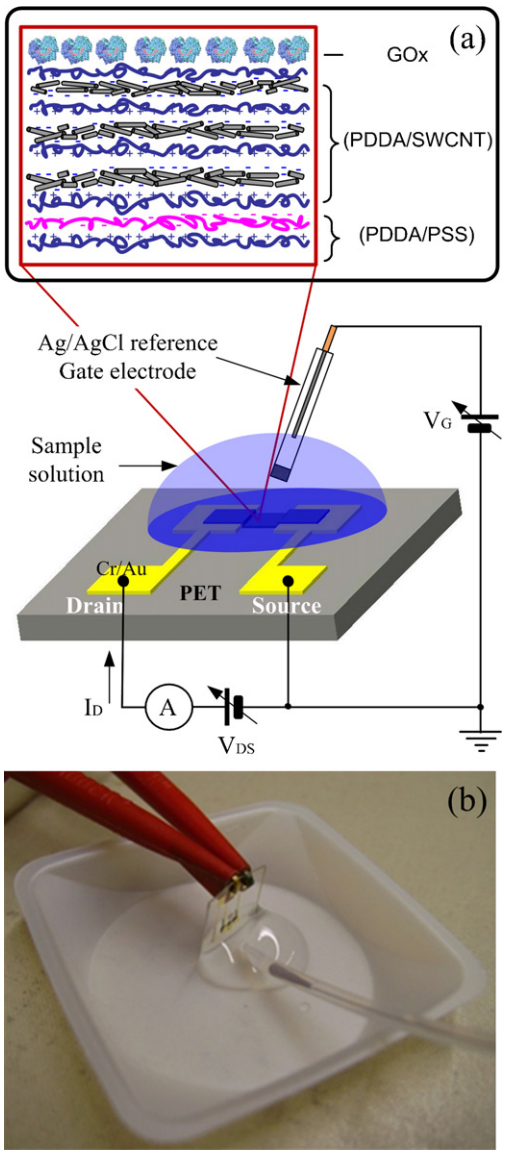

Fig. 2. The schematic diagram of the fabricated flexible SWCNT ISFET sensors with characterization scheme for pH/glucose sensing: (a) Vertical hierarchical structure of multilayer thin film for sensing with ISFET testing method, and (b) a photograph of experimental testing set-up with an external Ag/AgCl reference electrode.

The Ag/AgCl reference gate electrode and the readout wires from source and drain electrode were fixed to the external frame to prevent the relative motion. At this time the distance between sensor surface and the tip of reference electrode was about 5 mm. And a pipette was used to add 300 μL of sample solution on the sensor surface with reference electrode immersed. The sensors were incubated in each pH buffer solution for 1 min. A longer incubation time, 3 min was used for glucose sensing on the consideration of glucose enzyme retention time and ionic diffusion of reactants and products. V_{DS} was scanned from 0 to −1.0 V with a step of −20 mV and V_G was swept from 0 to −1.5 V with a step of −0.3 V. The used sample solution was sucked and the sensor surface was washed with DIH_2O several times between measurements without repositioning of reference electrode.

The time response measurement was conducted differently from ISFET characterization of pH and glucose. The conductance of the LbL SWCNT multilayer was collected using Data logging/switch system (Agilent 34970A) without the reference electrode. After the acquisition in one pH buffer, the used buffer was sucked and new pH buffer was applied without rinsing sensor surface.

3. Results and discussions

3.1. Flexible SWCNT ISFETs

The fabricated standard 4 in. wafer level devices and diced individual chips are shown in Fig. 3a and b, respectively. SWCNT terminated surface was characterized with field emission gun scanning electron microscope (FE-SEM, Jeol 6500). SWCNTs are selectively assembled only on the channel area which is 10 μm long and 1 mm wide, as shown in Fig. 3c. The magnified SEM image of an SWCNT film on the channel is shown in Fig. 3d where random SWCNTs network is observed.

The fabrication was performed with freestanding flexible PET substrates that are identical in size to the standard 4 in. wafer without attaching it to flat wafers as described elsewhere (Liu et al., 2007; Xue and Cui, 2008a). Furthermore, multiple lithographic techniques were used due to the chemical and thermal resistance of PET polymer. The fabricated flexible SWCNT ISFET in this study features the absence of the inorganic dielectric layer such as SiO_2, Si_3N_4, Al_2O_3, or Ta_2O_5, etc., which has played a role of the receptor or donor of charge carriers in the traditional ISFET. Instead, SWCNTs play a role of inorganic dielectric layer using abundant carboxylic groups on SWCNTs surface. Therefore, variation of the surface charge induced by the shift in ionic composition directly influences the conductance of semiconducting SWCNT layers (Lee and Cui, 2009b).

On the other hand, a series of nanomaterial-based ISFET sensors developed (Liu et al., 2007; Xue and Cui, 2008b) held silica nanoparticles as a dielectric layer, which collects charge carriers on the surface, resulting in the conductance change in underlying semiconducting layer. However, the penetration of ion species into the semiconducting nanomaterial layer is significant, which would cause the change in electrical properties of the nanomaterial itself due to protonation/deprotonation and/or the proximal ionic composition (Kwon et al., 2006; Lee and Cui, 2009b). This dual effect of charge carriers on the conductance of semiconducting nanomaterials makes it difficult to analyze behaviors of nanomaterial-based ISFET sensors. For example, the decrease in pH in the sample solution causes a less negative gate voltage effect through protonation of hydroxyl groups on the gate dielectric nanoparticles, which might be the adverse effect to conductance increase in p-type semiconducting SWCNTs. Besides, we recently demonstrated carboxylated SWCNTs themselves carried pH-dependent conductance (Lee and Cui, 2009a,b), which suggests the elimination of gate dielectric layer for the construction of SWCNT-based ISFET sensors. Therefore, the multilayer structures of $(PDDA/PSS)_3(PDDA/SWCNT)_3$ and additional $(PDDA/GOx)_3$ were used for pH/glucose sensing in this study, respectively.

3.2. Flexible SWCNT ISFETs for pH sensing

First of all, the flexible SWCNT ISFET pH sensor was characterized at pH 5 buffer to demonstrate a basic functionality of transistors (Supplementary Fig. 2). The explicit field-effect and gate transfer characteristics demonstrated that SWCNTs are p-type semiconducting materials. As V_G increases, the conductance of SWCNT multilayer increases, thereby yielding increasing I_D. Furthermore, the saturation effects are observed above $V_G = -0.6$ V below which the ionic conductor behavior is observed above $V_{DS} = -0.8$ V. The effect of the ionic conductor was observed significantly in the SWCNTs resistors (Lee and Cui, 2009a,b). It means that the high negative gate voltage localizes positively charged ions, suppressing the ionic conducting effect. At low gate voltage, however, V_{DS} plays a dominant role of driving charged species for ionic conductor. The reason for the positive $V_{th} = 0.8$ V for p-type semiconductor and low $I_{on/off} = 3.8$ is the presence of metallic

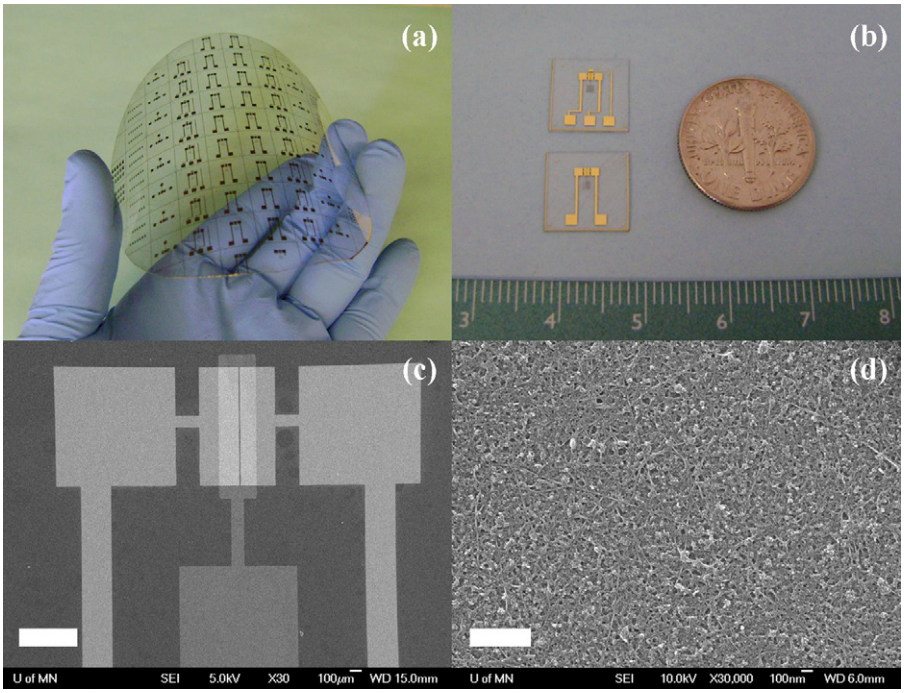

Fig. 3. A fabricated flexible SWCNT ISFET sensor: (a) standard 4 in. wafer level devices with a demonstrative bending, (b) 1 cm × 1 cm individual chips, (c) an SEM image of microfabricated electrodes and nano-assembled SWCNT film in channel area (scale bar: 500 μm), and (d) a magnified SEM image of SWCNT film in channel area (scale bar: 500 nm).

SWCNTs in the LbL assembled film, which allows current flow even though semiconducting SWCNTs are in off-state. The charged ions dissolved in pH buffers may deteriorate the positive V_{th} and low $I_{on/off}$. Nevertheless, SWCNTs ISFET sensors are still useful for chemical and biological sensors, since the ion-responsive electrical signals are obtained. The gate leakage current was less than 1 μA under $V_G = -1.5$ V and $V_{DS} = 0$ V, which is remarkably smaller than the reported one in previous SWCNTs ISFET sensors (Xue and Cui, 2008b), where Ag/AgCl wire without the electrolyte was used as a reference electrode. By exposing wire surface to sample solution, there might be side electrochemical reaction, which can be seen as gate leakage current that resulted in failure to providing the stable solution potential (Minot et al., 2007). By using the internal filling solution of 3 M KCl, low gate leakage current 1300 times smaller than I_D at the highest V_{DS} and V_G tested was obtained. For comparison, the reported one (Xue and Cui, 2008b) was 10 times smaller than I_D at the highest V_{DS} and V_G tested.

The pH response of the fabricated flexible SWCNT ISFET sensor is also shown in Fig. 4. It is apparently observed in Fig. 4a that higher current flows at a lower pH at the fixed $V_G = -1.5$ V throughout the V_{DS} tested. In SWCNT resistors (Lee and Cui, 2009a,b) where the gate electrode was not used, *I*–*V* was in parabolic relationship. In ISFETs, however, saturation effects are found in I_D due to the gate voltage, which localizes charged ions and suppresses the ionic current as mentioned. The I_D at the fixed $V_{DS} = -1.0$ V and $V_G = -1.5$ V were extracted and redrawn versus pH in Fig. 4b. The current is exponentially dependent on pH, which indicates that molecular protonation/deprotonation plays a role of the electrical property change in SWCNTs (Lee and Cui, 2009b). The I_D at the fixed $V_{DS} = -1.0$ V and $V_G = -1.5$ V were normalized by the current at pH 7, since current levels from devices in one batch were different due to the difference in initial conductance of SWCNT ISFETs caused by the random network of SWCNTs. Eight devices with 10 μm channel length were tested and currents were normalized. $I_D/I_{D,pH7}$ versus pH curve is shown in Fig. 4b. The time response of the SWCNT multilayer conductance to pH buffers without the gate voltage applied is shown in Fig. 4c. In the atmosphere where the conductance of SWCNTs is susceptible to micro-environment such as ambient air flow and wetting status, the conductance is in transition. However, once the pH buffer solution is applied, the conductance of the

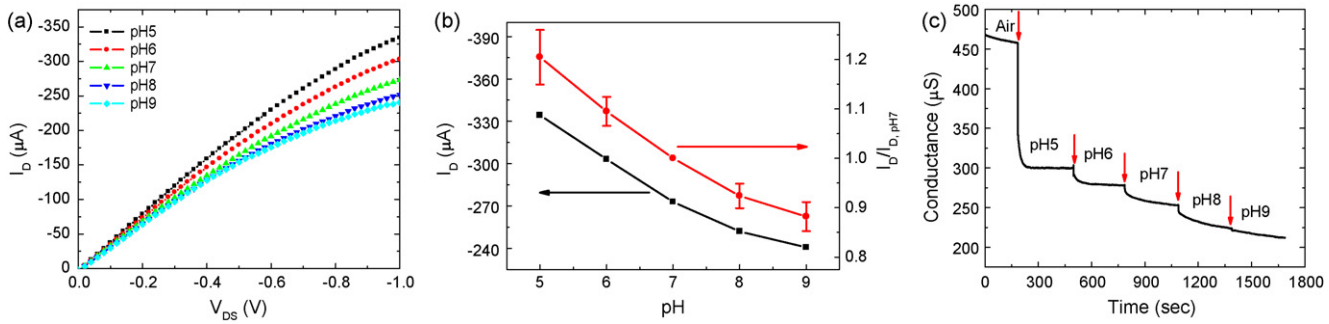

Fig. 4. The pH response of the fabricated flexible SWCNT ISFET sensor: (a) representative drain current (I_D)–voltage (V_{DS}) curves funder different pH buffers at fixed $V_G = -1.5$ V, (b) pH-responsive drain current and normalized I_D by the current at pH 5 buffer from 8 devices tested at fixed $V_{DS} = -1.0$ V and $V_G = -1.5$ V, and (c) time response of the flexible SWCNT multilayer conductance to pH without gate voltage applied.

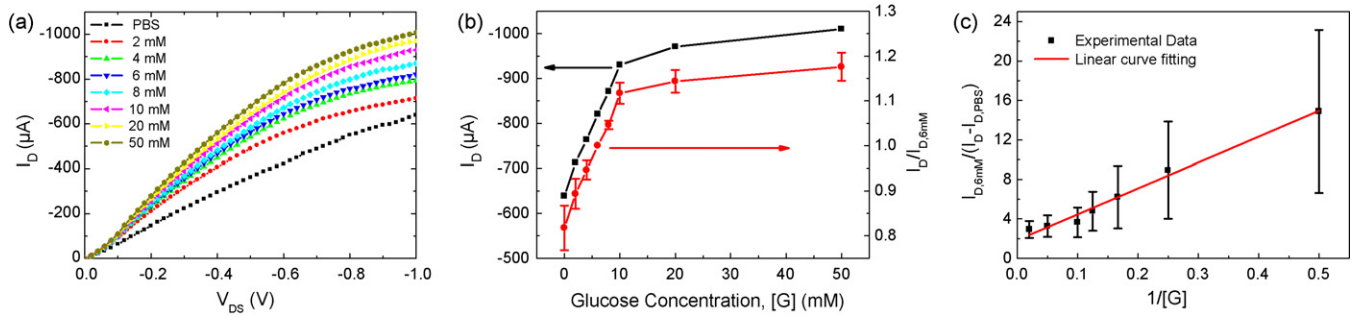

Fig. 5. Glucose concentration test using the flexible SWCNT ISFET sensor with the layer of $(PDDA/PSS)_2(PDDA/SWCNT)_3(PDDA/GOx)_3$: (a) representative drain current (I_D)–voltage (V_{DS}) curves in different glucose concentrations at fixed $V_G = -1.5$ V, (b) glucose-responsive drain current (I_D) and normalized I_D by the current at 6 mM from 7 devices tested at fixed $V_{DS} = -1.0$ V and $V_G = -1.5$ V, and (f) Lineweaver–Burk plot of ΔI_D^* and glucose concentration [G].

SWCNT multilayer decreases exponentially, followed by the stabilization with the time constant of within 1 min. This pH-dependent conductance without the gate reference electrode implies that the local pH in the proximity of SWCNTs plays a role of the substitutive gate voltage which is ameliorated by external electric voltage.

3.3. Flexible SWCNT ISFETs for glucose sensing

The basic functionality of the flexible SWCNT ISFETs with $(PDDA/PSS)_3(PDDA/SWCNT)_3(PDDA/GOx)_3$ at 10 mM glucose concentration was tested (Supplementary Fig. 3). A field-effect was also clearly observed and reveals that SWCNTs are p-type semiconducting materials. The gate transfer characteristic showed V_{th} of 1.1 V and $I_{on/off}$ of 2.7, which were different from those in pH sensing at fixed $V_{DS} = -1.0$ V presumably due to the sample solution used and the mutation in electrochemical properties of SWCNTs by additional GOx layers. The leakage current was less than 1.6 μA over the entire V_G range tested, which was 740 times smaller than I_D at the highest V_{DS} and V_G tested.

The flexible SWCNT ISFETs were tested in various glucose concentrations. The glucose-responsive flexible sensor behaviors are shown in Fig. 5. I_D increases with increase in glucose concentration at fixed $V_G = -1.5$ V over the entire V_{DS} tested as shown in Fig. 5a. The glucose-responsive I_D from one device at fixed $V_{DS} = -1.0$ V and $V_G = -1.5$ V is depicted in Fig. 5b, where a sensitivity of 28.4 μA/mM was found on the linear range of 2–10 mM. Seven devices with 10 μm channel length were tested for glucose sensing, and currents were normalized with the current at the glucose concentration of 6 mM. $I_D/I_{D,6\,mM}$ versus glucose concentration curve was added in Fig. 5b. Generally, sensitivities were found as the range of 18–45 μA/mM due to the initial conductance variance of devices themselves even though all devices tested showed a linear range of 2–10 mM. This fact suggests the possibility of the physiological glucose diagnostics with the normalization scheme. The sensitivities found were larger than the ones reported for planar devices (Lee and Cui, 2009a; Liu and Cui, 2006; Zhu et al., 2002). The reasons for a higher sensitivity are attributed to: (1) the use of ISFET characterization method, where gate voltage influences on the oxidation of hydrogen peroxide (H_2O_2) to generate two more hydrogen ions and one electron per glucose molecule, and (2) use of flexible polymer substrate, where the bioactivity of immobilized enzyme can be retained. It is evident that the exponential dependence of I_D on pH resulted in linear dependence on glucose due to a log scale nature of pH (Lee and Cui, 2009a) at the low concentration of glucose.

However, it is noticeable that the saturation is clearly observable above 10 mM due to enzyme limited reactions. The reaction rate in Michaelis–Menten kinetics of the enzyme corresponds to the current flow in the electrochemical sensors, which can be considered as the hydrogen ion production rate in SWCNT ISFETs. A new reaction rate ΔI_D^* is defined as follows on the consideration of the normalization:

$$\Delta I_D^* = \frac{I_D - I_{D,PBS}}{I_{D,6\,mM}}$$

where $I_{D,PBS}$ is drain current at PBS and $I_{D,6\,mM}$ drain current at 6 mM glucose. Subsequently, Lineweaver-Burk plot is constructed as shown in Fig. 5c between ΔI_D^* and glucose concentration, [G] based on the following equation.

$$\frac{1}{\Delta I_D^*} = \frac{K_m^{app}}{\Delta I_{D\max}^*[G]} + \frac{1}{\Delta I_{D\max}^*}$$

where K_m^{app} is the apparent Michaelis–Menten constant, and $\Delta I_{D\max}^*$ corresponds to the maximum rate of the reaction. The derived K_m^{app} of 14.2 mM is considerably lower than free GOx (Silva et al., 1990), and comparable to reported results for other CNT-based glucose sensors (Chen et al., 2008; Wang et al., 2008), indicating a high affinity of LbL assembled GOx multilayer to glucose. In other words, LbL assembly of GOx on the CNT multilayer preserves the bioactivity.

The comprehensive glucose sensing mechanism in SWCNT ISFET sensors is illustrated in Fig. 6. β-D-Glucose is oxidized to D-glucono-δ-lactone with the catalysis reaction of GOx, followed by the hydrolysis of D-glucono-δ-lactone and the electrooxidation of H_2O_2 under applied gate potential to produce hydrogen ions as well as

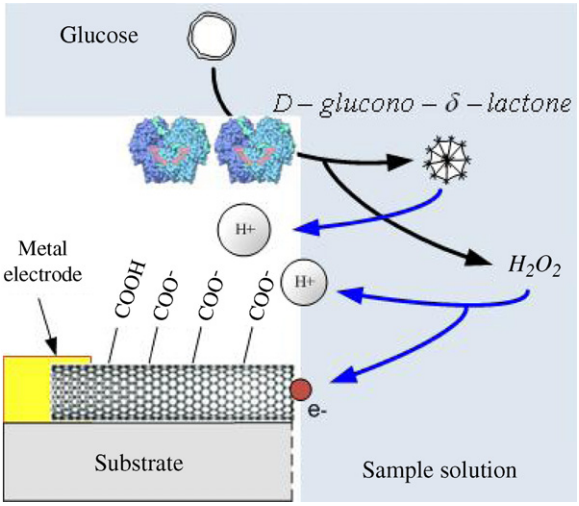

Fig. 6. A suggested comprehensive glucose sensing mechanism in SWCNT ISFET sensors.

electrons as follows.

$$\beta\text{-D-glucose} + O_2 \xrightarrow{GOx} \text{D-glucono-}\delta\text{-lactone} + H_2O_2$$
$$\text{D-glucono-}\delta\text{-lactone} + H_2O \rightarrow \text{D-gluconate}^- + H^+$$
$$H_2O_2 \xrightarrow{+0.7\,V} O_2 + 2H^+ + 2e^-$$

The electrical conductance change in SWCNTs can be caused by: (1) the proximal ionic composition change, and (2) direct electron transfer. The local pH change in the vicinity of SWCNTs and the direct electron transfer play the role of drain current change in the SWCNTs layer. Particularly, once the steady state reaches from the initial hydrogen ion depletion mode due to negative gate voltage applied, the concentration of hydrogen ions produced from glucose breakdown is maintained constant in the vicinity of GOx layer from which ions diffuse away to reach SWCNT transducer layer or disappear towards the bulk solution due to the buffering power of the sample solution. Therefore, the ionic composition in the proximity of SWCNTs results in pH changes, thereby the conductance change of SWCNTs. On the other hand, the direct electron transfer might take place from glucose directly to SWCNT surface due to applied gate voltage and/or drain-to-source voltage. Transferred electrons flow through SWCNT layer and contribute to the drain current.

4. Conclusions

In conclusion, we have investigated the fabrication of flexible SWCNT ISFET sensors using all lithographic techniques with LbL bottom-up construction, which makes the final product cost-effective due to the inexpensive polymer substrate and mass production. In addition, the flexible polymer substrate is biocompatible due to the material nature, which eliminates the need of dielectric layer, and makes *in vivo* application promising. The pH has been characterized based on the molecular protonation/deprotonation of carboxylated SWCNTs to show exponential decrease in drain current with increase in pH. Glucose has also been detected by the local pH change with the aid of bio-receptors, glucose oxidase (GOx) multilayer. The field-effects at pH 5 buffer and 10 mM glucose are significantly observed. Although V_{th} and $I_{on/off}$ are not as high as in solid-state devices, flexible SWCNT ISFETs have been proven to be useful for chemical and biological sensors. The sensors have shown low leakage currents due to the use of the Ag/AgCl reference gate electrode, which blocks ionic movements. Generally, glucose ISFETs have a sensitivity of 18–45 μA/mM on the linear range of 2–10 mM, and follow Michaelis–Menten kinetics. The derived Michaelis–Menten was 14.2 mM, indicating a high affinity of LbL assembled GOx to glucose. The LbL assembly of nanomaterials and enzymes on the transparent and flexible substrate suggests various chemical and biological sensors suited for *in vivo* applications.

Acknowledgments

This work was partially supported by the DARPA M/NEMS Science and Technology Fundamentals Research Program through the Micro/Nano Fluidics Fundamentals Focus (MF3) Center. The authors would like to acknowledge the Nanofabrication Center and Characterization Facility at the University of Minnesota, which are supported by NSF through NNIN.

Appendix A. Supplementary data

Supplementary data associated with this article can be found, in the online version, at doi:10.1016/j.bios.2010.03.003.

References

Bock, K., 2005. Proc. IEEE 93 (8), 1400–1406.
Chen, X., Chen, J., Deng, C., Xiao, C., Yang, Y., Nie, Z., Yao, S., 2008. Talanta 76 (4), 763–767.
Fujimoto, K., Fujita, S., Ding, B., Shiratori, S., 2005. Jpn. J. Appl. Phys. 44, L126–L128.
Han, J., 2004. In: Meyyappan, M. (Ed.), Carbon Nanotubes: Science and Application. CRC Press, New York, pp. 8–24.
Jiang, C., Tsukruk, V.V., 2006. Adv. Mater. 18 (7), 829–840.
Kwon, J.-H., Lee, K.-S., Lee, Y.-H., Ju, B.-K., 2006. Electrochem. Solid-State Lett. 9 (9), H85–H87.
Lee, D., Cui, T., 2009a. IEEE Sens. J. 9 (4), 449–456.
Lee, D., Cui, T., 2009b. J. Vac. Sci. Technol. B 27, 842–848.
Liu, Y., Cui, T., 2006. Sensor Lett. 4 (3), 241–245.
Liu, Y., Erdman, A.G., Cui, T., 2007. Sens. Actuat. A Phys. 136 (2), 540–545.
Loh, K.J., Kim, J., Lynch, J.P., Kam, N.W.S., Kotov, N.A., 2007. Smart Mater. Struct. 16, 429–438.
Mamedov, A.A., Kotov, N.A., Prato, M., Guldi, D.M., Wicksted, J.P., Hirsch, A., 2002. Nat. Mater. 1 (3), 190–194.
Minot, E.D., Janssens, A.M., Heller, I., Heering, H.A., Dekker, C., Lemay, S.G., 2007. Appl. Phys. Lett. 91 (9), 093507.
Nohria, R., Khillan, R.K., Su, Y., Dikshit, R., Lvov, Y., Varahramyan, K., 2006. Sens. Actuat. B Chem. 114 (1), 218–222.
Rouse, J.H., Lillehei, P.T., 2003. Nano Lett. 3 (1), 59–62.
Shutava, T.G., Kommireddy, D.S., Lvov, Y.M., 2006. J. Am. Chem. Soc. 128 (30), 9926–9934.
Silva, M.A.D., Beddows, C.G., Gil, M.H., Guthrie, J.T., Guiomar, A.J., Kotov, S., Piedade, A.P., 1990. Radiat. Phys. Chem. 35 (1–3), 98–101.
Wang, Y., Wang, X., Wu, B., Zhao, Z., Yin, F., Li, S., Qin, X., Chen, Q., 2008. Sens. Actuat. B Chem. 130 (2), 809–815.
Xue, W., Cui, T., 2008a. Sens. Actuat. A Phys. 145–146, 330–335.
Xue, W., Cui, T., 2008b. Sens. Actuat. B Chem. 134 (2), 981–987.
Yu, H., Cao, T., Zhou, L., Gu, E., Yu, D., Jiang, D., 2006a. Sens. Actuat. B Chem. 119 (2), 512–515.
Yu, X., Rajamani, R., Stelson, K.A., Cui, T., 2006b. Sens. Actuat. A Phys. 132 (2), 626–631.
Zeng, T., Claus, R., Zhang, F., Du, W., Cooper, K.L., 2001. Smart Mater. Struct. 10, 780–785.
Zhu, J., Zhu, Z., Lai, Z., Wang, R., Guo, X., Wu, X., Zhang, G., Zhang, Z., 2002. Sensors 2 (4), 127–136.